NeuroImage 179 (2018) 530–539

Contents lists available at ScienceDirect

NeuroImage

journal homepage: www.elsevier.com/locate/neuroimage

Effect sizes of BOLD CVR, resting-state signal fluctuations and time delay measures for the assessment of hemodynamic impairment in carotid occlusion patients

Jill B. De Vis [a,*], Alex A. Bhogal [b], Jeroen Hendrikse [b], Esben T. Petersen [b,c], Jeroen C.W. Siero [b,d]

[a] National Institute of Health (NIH) / National Institute of Neurological Disorders and Stroke (NINDS), Bethesda, MD, USA
[b] Department of Radiology, University Medical Centre Utrecht, Utrecht, The Netherlands
[c] Danish Research Centre for Magnetic Resonance, Hvidovre Hospital, Denmark
[d] Spinoza Centre for Neuroimaging Amsterdam, Amsterdam, the Netherlands

ARTICLE INFO

Keywords:
Magnetic resonance imaging
MRI
Blood oxygen level dependent
BOLD
Brain
fMRI
Resting-state fMRI
Cerebrovascular reactivity
Cerebrovascular disease

ABSTRACT

Background and purpose: The BOLD signal amplitude as a response to a hypercapnia stimulus is commonly used to assess cerebrovascular reserve. Despite recent advances, the implementation remains cumbersome and alternative ways to assess hemodynamic impairment are desirable. Resting-state BOLD signal fluctuations (rsBOLD) have been proposed however data on its sensitivity and dependence on baseline venous cerebral blood volume (vCBV) is limited. The primary aim of this study was to compare the effect sizes of resting-state and hypercapnia induced BOLD signal changes in the detection of hemodynamic impairment. The second aim of the study was to assess the dependence of BOLD signal variability on vCBV.

Materials and methods: Fifteen patients with internal carotid artery occlusive disease and 15 matched healthy controls were included in this study. The BOLD signal was derived from a dual-echo gradient-echo echo-planar sequence during hypercapnia (HC) and hyperoxia (HO) gas modulations. BOLD (fractional) amplitude of low frequency fluctuations ((f)ALFF) was compared to HC-BOLD, BOLD response delays derived from time delay analysis and ΔBOLD in response to progressively increasing HC. Effect sizes (i.e. the standard mean difference between patients and controls) were calculated. HO-BOLD was used to estimate vCBV, and its contribution to the variability in rsBOLD signal was evaluated.

Results: The effect sizes of ALFF and fALFF (0.61 and 0.72) were lower than the effect sizes related to hypercapnia-based hemodynamic assessment analysis; 1.62, 1.56 and 0.90 for HC-BOLD, BOLD response delays and ΔBOLD in response to progressively increasing HC. A moderate relation was found between (f)ALFF and HC-BOLD in controls (R^2 of 0.61 and 0.42), but this relation decreased in patients (R^2 of 0.33 and 0.15). (f)ALFF did not differ between patients and controls whereas HC-BOLD did ($p < 0.005$). The ΔBOLD response to progressively increasing HC was significantly different in between patients and controls for $\Delta EtCO_2$ values $\geq$ 2 mmHg (at +2 mmHg $F(1, 18) = 5.85$, $p = 0.026$). Up to 31% and 53% of the variance in the ALFF and HC-BOLD spatial distribution could be explained by HO-BOLD.

Conclusion: ALFF and fALFF demonstrated a moderate effect size to detect hemodynamic impairment whereas the effect size was large for methods employing a hypercapnia-based vascular stress stimulus. Based on our analysis of BOLD signal change as a response to a progressively increasing hypercapnia stimulus we can argue that a hypercapnia stimulus of at least 2 mmHg above baseline $EtCO_2$ is necessary to evaluate hemodynamic impairment. We also demonstrated that a substantial amount of information imbedded in the rsBOLD and HC-BOLD was explained by HO-BOLD. HO-BOLD can serve as a proxy for vCBV and this thus indicates that one should be careful when adopting these techniques in disease cases with compromised CBV.

* Corresponding author. National Institute of Health (NIH) / National Institute of Neurological Disorders and Stroke (NINDS), Building 10, Room B1D733, 10 Center Drive, Bethesda, MD, 20892, USA.

E-mail addresses: jill.devis@nih.gov (J.B. De Vis), a.bhogal@umcutrecht.nl (A.A. Bhogal), j.hendrikse@umcutrecht.nl (J. Hendrikse), esbentp@drcmr.dk (E.T. Petersen), j.c.w.siero@umcutrecht.nl (J.C.W. Siero).

https://doi.org/10.1016/j.neuroimage.2018.06.017
Received 5 March 2018; Received in revised form 1 June 2018; Accepted 5 June 2018
Available online 18 June 2018

Abbreviations

ΔEtO2	Difference in EtO2 from baseline to hypercapnia
ΔEtCO2	Difference in EtCO2 from baseline to hypercapnia
ALFF	Amplitude of low frequency fluctuations
ASL	Arterial spin labeling
BOLD	Blood oxygen level-dependent
CBF	Cerebral blood flow
CO2	Carbon dioxide
CSF	Cerebrospinal fluid
CVR	Cerebrovascular reserve
DSC	Dynamic susceptibility contrast
EtO2	End-tidal partial pressure of oxygen
EtCO2	End-tidal partial pressure of carbon dioxide
fALFF	Fractional amplitude of low frequency fluctuations
FLIRT	FMRIB's linear image registration tool
FSL	FMRIB's software library
GM	Gray matter
HC	Hypercapnia
HC-BOLD	Hypercapnia induced blood oxygen level-dependent signal changes
HO	Hyperoxia
HO-BOLD	Hyperoxia induced blood oxygen level-dependent signal changes
ICA	Internal carotid artery
MNI	Montreal neurological institute
MP-RAGE	Magnetization prepared rapid acquisition echo
MRI	Magnetic resonance imaging
Ns	Non-significant
O2	Oxygen
PaCO2	Arterial partial pressure of carbon dioxide
pCASL	Pseudocontinuous arterial spin labelling
PLD	Postlabel delay
ROI	Region of interest
rsBOLD	Resting-state blood oxygen level-dependent signal
VASO	Vascular space occupancy
vCBV	Venous cerebral blood flow

Introduction

The brain maintains stable cerebral blood flow by autoregulation and adapting its vascular reserve (Derdeyn et al., 1999). These compensatory responses encompass cerebrovascular reserve capacity (CVR) and are mainly achieved by smooth muscle relaxation or contraction. An impairment in CVR has been associated with an increased risk of cerebrovascular disease (Blaser et al., 2002; Yonas et al., 1993; Kuroda et al., 2004; Markus and Cullinane, 2001), to an increased microbleed load (Conijn et al., 2012) and cortical thinning (Fierstra et al., 2010), and has consequences for patient management (Poublanc et al., 2011). CVR can be assessed by administrating a vascular stress agent; either by modulating the arterial partial pressure of carbon dioxide ($PaCO_2$) (Poulin et al., 1996; Mark et al., 2010) or by administering a carbonic anhydrase inhibitor such as acetazolamide (ACZ) via injection. Magnetic resonance imaging (MRI) techniques such as arterial spin labelling (ASL) and blood oxygen level-dependent (BOLD) allow for non-invasive measurements of CVR with high spatial resolution and coverage and adequate temporal resolution. Although, a previous study did show BOLD CVR to be more sensitive to hemodynamic impairment then ASL CVR (De Vis et al., 2015a).

The implementation of CVR mapping using gas manipulations is subjected to several considerations, for instance time pressure constraints, medical ethical concerns, the availability of the gas modulation devices, and importantly the tolerability of the patient group to the vascular stress stimulus. CVR is commonly assessed by looking at the BOLD signal amplitude during hypercapnia, administered using a simple block design, however, also more elaborate stimuli have been explored such as a progressively increasing ramp (Sobczyk et al., 2014; Bhogal et al., 2016; Donahue et al., 2014; Spano et al., 2013).

Recently, BOLD MRI resting-state signal fluctuations (rsBOLD) have been proposed as an alternative means for the assessment of cerebral hemodynamics, i.e. CVR (Golestani et al., 2016; Kannurpatti et al., 2014; Jahanian et al., 2014, 2016). The inspiration of applying rsBOLD techniques for the assessment of hemodynamic impairment was based on results reporting that baseline BOLD signal variation contained physiological signal components such as blood pulsation and respiratory-induced changes in $PaCO_2$ (Biswal et al., 2007; Biswal and Kannurpatti, 2009; Kannurpatti et al., 2008; Tong and Frederick, 2010). Non-neuronal fluctuations in hemodynamic parameters were shown to account for ~30% of the variance in gray matter BOLD signal fluctuations (Frederick et al., 2012), and fluctuations in $PaCO_2$ were shown to have a strong influence, up to ~16% of the variance in significant voxels (Wise et al., 2004), on the rsBOLD signal (Golestani et al., 2016; Wise et al., 2004; Chang and Glover, 2009). Although rsBOLD probes more subtle vascular dynamics compared to a BOLD measure of hypercapnic responses, the results of the first few studies applying rsBOLD MRI for hemodynamic impairment assessment have been encouraging (Golestani et al., 2016; Kannurpatti et al., 2014; Jahanian et al., 2014; Lipp et al., 2015). However, studies evaluating the rsBOLD for hemodynamic impairment assessment in patient populations are scarce (Liu et al., 2017a).

Besides BOLD signal amplitude, also the BOLD signal delay time during hypercapnia can be used to probe cerebral hemodynamics (Christen et al., 2015a). The BOLD delay time is thought to depend both on the arrival of blood, i.e. arterial transit time, and the time it takes the vasculature to respond to the elevated $PaCO_2$, i.e. reaction time. As BOLD delay time assessment provides us with two important measures of cerebrovascular health, the technique has gained increasing attention (Christen et al., 2015b; Cogswell et al., 2017; Liu et al., 2017b; Donahue et al., 2015; Champagne et al., 2017).

The primary aim of this study was to compare the different proposed measures of BOLD-MRI-based hemodynamic assessment. In particular, their utility in the assessment of hemodynamic impairment in patients with carotid occlusion was investigated. In these patients, blood flow through the carotid artery is interrupted. This does not necessary lead to a perfusion deficit but may result in a dilatory response of some of the remaining brain-feeding arteries resulting in a decreased vascular reserve within that area. For our primary aim, effect sizes of BOLD hemodynamic assessment methods relying on the resting-state signal fluctuations, specifically the BOLD signal amplitude of low-frequency fluctuations (ALFF) (Biswal et al., 1995; Zang et al., 2007; Yang et al., 2007) and the fractional ALFF (fALFF) (Zou et al., 2008), were calculated and compared against BOLD hemodynamic assessment methods relying on a vascular stress stimulus. For the latter, effect sizes of block-design, hypercapnia-based CVR (HC-BOLD) (Donahue et al., 2015), BOLD delay time heterogeneity (Donahue et al., 2015), and BOLD signal change as a response to a progressively increasing hypercapnic stimulus (Bhogal et al., 2016) were evaluated. The second aim of this study was to investigate the contribution of baseline venous CBV (vCBV) to the BOLD signal variability to explore the notion that the BOLD signal changes are partly determined by baseline vCBV as predicted by basic BOLD biophysical models (Davis et al., 1998; Ogawa et al., 1993). This is of importance when attributing BOLD signal amplitude fluctuations solely to neuronal activity or as a proxy for $PaCO_2$-related changes in vascular dynamics. In this assessment, adopting previously-made assumptions,

hyperoxia induced BOLD signal changes (HO-BOLD) were taken as a proxy for the vCBV (Liu et al., 2017b; Bulte et al., 2007).

Materials and methods

Subjects

This study was approved by our local institutional review board under protocol number 'NL 39070.041.11' and conformed to the standards set by the latest revision of the declaration of Helsinki. Patients with currently asymptomatic occlusive disease of the internal carotid arteries (ICA) and age-and gender matched healthy controls were included in this study. Fifteen currently asymptomatic (for 9 ± 4 years) patients (14 male/1 female) with unilateral or bilateral (3 subjects) ICA occlusion were included. Of these 15 patients, MR imaging could not be completed in 4 patients; 2 patients suffered from claustrophobia and another 2 experienced anxiety during the hypercapnia challenge. A fifth patient had to be excluded due to excessive motion artefacts. Therefore, only data of 10 of the 15 included subjects could be used for final data-analyses and those 10 subjects were matched based on age-and gender to ten included healthy controls. Subjects were defined as healthy if no previous history of cerebrovascular disease or other brain disease was present, and if no structural lesions were seen (conventional MRI) and no evidence of steno-occlusive disease of the brain-feeding arteries was present (MR angiography). Signed informed consent was obtained from all participants in this study. Part of the data obtained in this study has been described earlier (De Vis et al., 2015b).

Study design

In the included subjects, an in-house built dual-echo pseudo-continuous arterial spin labelling (pCASL) sequence was performed under hypercapnic (HC) and hyperoxic (HO) gas modulations. The following maps were generated based on the acquired data; BOLD amplitude of low frequency fluctuations (ALFF) maps (Biswal et al., 1995; Zang et al., 2007; Yang et al., 2007), fractional ALFF (fALFF) maps (Zou et al., 2008), HC- and HO-BOLD maps (in %BOLD and as z-score maps). As well, BOLD time delay analysis using the RapidTiDe method (Donahue et al., 2015) and BOLD signal change as a response to a progressively increasing hypercapnia stimulus were investigated. RsBOLD, HC-BOLD, time delay analysis and BOLD signal change in response to progressively increasing hypercapnia were used to compare effect sizes. HO-BOLD was used to evaluate the contribution of vCBV to (f)ALFF.

MR imaging

MR imaging was performed on a Philips 3 Tesla system using a quadrature body coil for transmission and an 8-channel head coil for reception (Achieva, Philips Medical Systems, Best, the Netherlands). A dual-echo pseudo-continuous arterial spin labelling (pCASL) sequence was performed. Scan parameters of the pCASL sequence were as follows: TR/TE1/TE2: 4000/13.79/36.25 ms, label duration: 1650 ms, postlabel delay (PLD): 1550–2185 ms (multi-slice readout resulted in varying PLDs), FOV: 240×240 mm^2, voxel dimensions: 3×3x7 mm^3, number of slices: 11, slice gap: 1 mm, SENSE factor: 2.3, echo train length: 35, volumes: 280, no background suppression, readout: multi-slice gradient-echo (GE) single-shot echo planar imaging (EPI), total scan duration: 18:30.

Respiratory paradigm

A computer-controlled prospective end-tidal gas targeting system (Respiract™, Thornhill Research Inc., Toronto, Canada) was used to modulate end-tidal carbon dioxide and oxygen partial pressures ($EtCO_2$ and EtO_2, respectively) (Slessarev et al., 2007). Gas modulations were applied via a breathing circuit sealed to the subject using transparent dressings (Tegaderm, 3M, St Paul, MN). Sample lines were connected from the breathing circuit to the RespirAct device which samples the partial pressures of CO_2 and O_2 at a rate of 40Hz. The gas-modulation paradigm was as follows; (1) baseline breathing (160s) after which the $EtCO_2$ was gradually ramped up (75s) to hypercapnia which was maintained at a plateau phase (105s) and followed by baseline breathing (70s), (2) hyperoxia breathing (180s), and (3) a repetition of the first block (i.e. $EtCO_2$ gradually (75s) ramped up from baseline to hypercapnia after which the $EtCO_2$ was kept at a stable hypercapnia level for 105s) and finishing off with a baseline period of 200s. A typical graph of the gas-modulation paradigm of one of the subjects is shown in Fig. 1. The average $EtCO_2$ and EtO_2 values which were recorded during baseline, hypercapnia, and hyperoxia breathing are shown in Table 1.

Data-analysis

Preprocessing of the BOLD MR images

To ensure a steady-state of the GE-EPI signal, the first four volumes were discarded. The remaining multi-echo data were combined using a contrast-to-noise weighted approach (Poser et al., 2006). The multi-echo combined interleaved label and control time series data were subsequently motion corrected using an affine or rigid transformation with 6 degrees of freedom (FMRIB's Linear Image Registration Tool – FLIRT, FMRIB's Software Library - FSL) whereby the mean image was taken as a reference image (Jenkinson et al., 2002; Jenkinson and Smith, 2001), linearly detrended (3dDetrend, software for Analysis and visualization of Functional magnetic NeuroImages, AFNI) (Cox, 1996) and spatially smoothed with a 5mm full-width at half-maximum (FWHM) Gaussian kernel (FMRIB's SUSAN, FSL) (Smith, 1997). The resulting interleaved label and control volumes were averaged using a sliding window of two volumes to generate BOLD time series data, this resulted in a temporal resolution of 4s. Table 1 shows the mean absolute translational motion and the image temporal noise-to signal ratio (tNSR = 1/tSNR*100%) for both subject groups. Considering the small mean absolute motion (<1mm) for both groups, we do not believe that motion artefacts significantly impacted image quality. The same is true for possible eddy currents effects, which we expect to be minimal due to the nature of the EPI gradients used. Moreover, eddy-current induced image distortions will manifest similarly in all volumes for both subject groups, and will, at worst, represent a systematic bias.

The EtO_2 and $EtCO_2$ traces recorded by the RespirAct were resampled to match the TR of the BOLD data (4s). BOLD timeseries from a preliminary gray matter (GM) segmentation (see 'Generating ROIs' sections below) was used in a correlation between the resampled $EtCO_2$ trace with the BOLD data. The point of maximum correlation was then used to temporally align the breathing data with the BOLD signal.

Generating HC and HO BOLD maps

Maps of hypercapnia (HC) and hyperoxia (HO) induced BOLD signal changes (%) and z-scores were computed using the normalized (between 0 and 1) shifted $EtCO_2$ and EtO2 traces as regressors in a general linear model (FMRI Expert Analysis Tool - Feat, FSL). The hypercapnia %BOLD data were normalized to each subject's average $\Delta EtCO_2$ or ΔEtO_2.

Generating maps of ALFF and fALFF

BOLD data were band-pass filtered (0.01–0.08 Hz) to remove very low-frequency drift and high-frequency physiological noise components such as (aliased) respiratory and cardiac induced fluctuations. ALFF maps were computed as the mean square root of the power spectrum in the 0.01–0.08 Hz frequency band for each voxel during the baseline periods (Zou et al., 2008). Before computing the ALFF index per voxel, the absolute BOLD signal was first normalized by the mean BOLD signal in the brain mask. For computing the fALFF index, the sum of the square root of the power in the 0.01–0.08 Hz frequency range was divided by the sum across the entire 0–0.125 Hz frequency range (Zou et al., 2008). This normalization purportedly suppresses physiological noise contributions

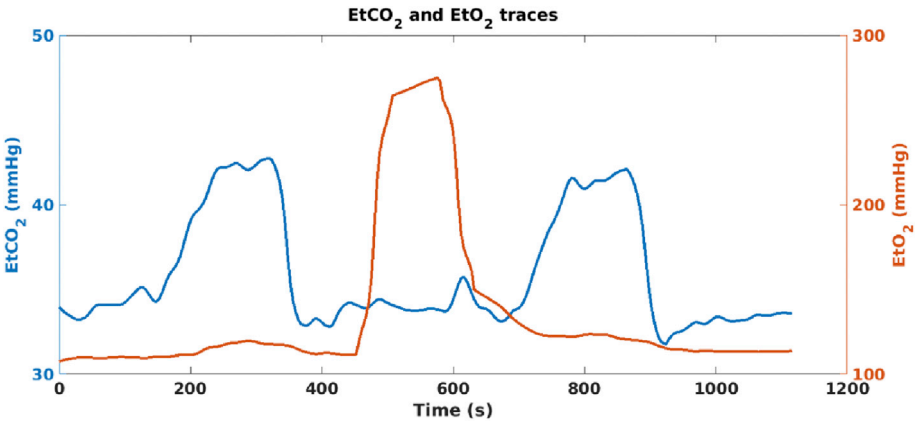

Fig. 1. Gas-modulation paradigm of one of the occlusion subjects who was included in this study. The gas-modulation paradigm consisted of three phases; (1) baseline breathing followed by a gradual increase in $EtCO_2$ which was then kept at a stable state for a while and followed by baseline breathing, (2) hyperoxia phase, and (3) repetition of the first block followed by a longer baseline period.

Table 1
Demographic data and end-tidal partial pressures of O2 and CO2 of healthy controls and currently asymptomatic patients with ICA occlusion.

	Controls	Occlusion patients
N	10	10
Male	8	9
Mean age ± sd (in years)	67 ± 5	65 ± 7
EtO_2 baseline (in mmHg)	114.9 ± 3.5	113 ± 3
$EtCO_2$ baseline (in mmHg)	35.4 ± 2.5	34.8 ± 1.5
EtO_2 hypercapnia (in mmHg)	122.3 ± 5.2	118.6 ± 2.7
$EtCO_2$ hypercapnia (in mmHg)	42.3 ± 2.4	40.8 ± 1.7
EtO_2 hyperoxia (in mmHg)	267.2 ± 26.5	251.4 ± 21.3
$EtCO_2$ hyperoxia (in mmHg)	36.0 ± 2.8	35.4 ± 1.6
Mean absolute motion (mm)	0.54 ± 0.17	0.47 ± 0.19
Image tNSR (%)	1.26 ± 0.15	1.18 ± 0.05
Baseline GM CBF (ml/100g/min)	41.1 ± 5.5	38.9 ± 6.4
Occlusion		
RICA		3
LICA		4
Double-sided		3
Previous symptoms		
Stroke		4
TIA		8
Amaurosis fugax		6
Time from symptoms to MRI[a]		
Mean ± sd (in years)		9 ± 5
Range (in years)		1–17

Sd, standard deviation; EtO_2, end-tidal partial pressure of oxygen; $EtCO_2$, end-tidal partial pressure of carbon dioxide; tNSR, temporal noise-to-signal metric (=1/tSNR*100%); GM CBF, gray matter cerebral blood flow; RICA, right internal carotid artery; LICA, left internal carotid artery; TIA, transient ischemic attack. This table shows the baseline and respiratory characteristics (mean ± sd) for the healthy controls and the patients with occlusive disease of the ICA. No significant differences were found between both groups. In addition, mean absolute motion, image tNSR and baseline GM CBF values did not differ significantly across groups. The correspondence in absolute motion and image tNSR between groups demonstrates the stability of the BOLD scan across groups.
Note that data is shown for subjects who were included in final data-analysis.
[a] Patients were asymptomatic at the time of MRI but did present with symptoms initially. The 'time from symptoms to MRI' gives the time interval between their initial symptomatic presentation and the research MRI study described in this paper.

from large blood vessels and cerebrospinal fluid (CSF) that affect the entire frequency spectrum.

Generating time delay maps

Time delay information of the BOLD signal was based on the Rapid-TiDe approach (Donahue et al., 2015). The entire dataset was used for this analysis, and the shifted $EtCO_2$ trace was used as probe regressor. This differs from the referred paper where lag time was calculated relative to the mean hemodynamic response. In this study, we chose not to relate the lagtime to the mean cerebral hemodynamic response as this would likely already be affected in carotid occlusion patients and would result in a diminished effect size of the time delay metrics. Per voxel, both the BOLD data and regressor time series were oversampled by a factor of 8 to improve estimation of the cross-correlation function, which was extracted over a -30–100s time range. Per subject, the kurtosis and variance of the time delay distribution (in gray and white matter) was computed as an index for time delay heterogeneity (Donahue et al., 2015).

BOLD signal change as a response to a progressively increasing stimulus

To assess the BOLD signal change as a response to a progressively increasing stimulus, the CO_2 components of the first gas-modulation block were isolated from the first stable hypercapnic period by manually selecting the starting and ending points of the progressively increasing CO_2 stimulus. The second hypercapnic period was not used in this analysis to avoid confounds relating to the effects of residual O_2/CO_2 on the BOLD signal response. CVR was expressed as the %BOLD signal change as a function of increases in $EtCO_2$, creating BOLD-CVR curves. For each subject, a sigmoidal response model was fit to the CVR response to generate BOLD-CVR response curves as described in (Bhogal et al., 2014, 2015). Next, BOLD-CVR curves of all subjects were shifted with respect to individual measured baseline $EtCO_2$ values (see methods Bhogal et al. [50]). This allowed us to express changes in CVR as a function of changes in $EtCO_2$ from baseline, thus, facilitating inter-subject averaging of the BOLD-CVR response to progressive hypercapnia.

Generating ROIs

All maps were registered to a 2mm Montreal Neurological Institute 152 (MNI-152) atlas (Mazziotta et al., 2001) using an affine transformation with FSL's FLIRT (Jenkinson et al., 2002). Gray and white matter ROIs were obtained from the Harvard-Oxford atlases for the MNI-152 2mm standard-space and the white matter ROI was eroded by one voxel to avoid partial volume effects with gray matter. Analysis of the HC/HO BOLD maps and of the ALFF/fALFF maps was performed using the whole brain gray matter ROIs. Analysis of the time delay maps and of the BOLD signal change as a response to a progressively increasing stimulus was performed using both the whole brain gray matter and the whole brain white matter ROIs.

Statistical analysis

One-sided Student's t-tests were used to assess the differences

between occlusion patients and controls in terms of ALFF, fALFF, HC-BOLD, HO-BOLD, and kurtosis and variance of time delay distribution.

The HC-BOLD response for progressively increasing $EtCO_2$ was analyzed using a three-way ($2 \times 2 \times 10$) mixed design ANOVA with the within- and between-subject factors of $EtCO_2$ (10 levels), tissue type (gray and white matter) and group type (patient, healthy control), respectively. As the Mauchly's test indicated that the assumption of sphericity was violated ($\chi 2(44) = 1735$, $p < 0.001$), we corrected the degrees of freedom using Greenhouse-Geisser estimates of sphericity ($\varepsilon = 0.18$). For all computed measured, standardized effect sizes (i.e. the difference between patients and controls in the mean of a measure, divided by the pooled standard deviation) were computed using Cohen's d. Statistical analysis was performed using SPSS 23.0 (IBM SPSS Statistics for Windows, Version 23.0. Armonk, NY: IBM Corp.). For all statistical tests, a p-value <0.05 was considered significant.

Results

Of the 15 patients with currently asymptomatic occlusive ICA disease, MRI could not be performed in 2 patients due to claustrophobia and in 2 patients due to anxiety evoked by hypercapnic breathing. Another one patient was excluded from all following analysis due to bad image quality. The mean age of the remaining 10 patients was 65 (±7, 52–73) year. The mean age of the 10 matched controls was 67 (±5, 60–76) year (Table 1). Of the remaining 10 patients, 3 patients had double-sided occlusion of their carotid arteries.

Results for a patient with a right ICA occlusion is shown in Fig. 2A. In this patient, the hemodynamic impairment is clearly visible by the interhemispheric differences in the HC-BOLD and time delay maps; the affected side shows substantial reduced HC-BOLD (%BOLD and z-value map) and prolonged time delays. For the HO-BOLD, ALFF and fALFF maps the impairment is not apparent. Plots of the BOLD signal response to a progressively increasing hypercapnia stimulus (Fig. 2B) demonstrate a clear reduction in the magnitude of the GM BOLD response in the hemisphere ipsilateral to the occluded artery. Compared with the contralateral hemisphere, the ipsilateral WM response was severely diminished (almost flat).

Fig. 3 shows the group average HC-BOLD, HO-BOLD, ALFF and fALFF maps for the occlusion patients (Fig. 3A) and healthy controls (Fig. 3B), respectively. A substantial reduced HC-BOLD is observed for the occlusion patients compared to the controls, whereas for the HO-BOLD, ALFF and fALFF maps any differences are not that clearly observable. Also, note the reduction in high values in large draining cortical vein areas for the z-value HC- and HO-BOLD maps. Fig. 4 shows boxplots of the group average results for gray matter HC-BOLD, HO-BOLD, ALFF and fALFF for the occlusion patients and healthy controls. Only significant differences were found for HC-BOLD, both for the %BOLD and z-score values, which were reduced for the occlusion patients.

The relationships between ALFF and HC-BOLD and HO-BOLD signal changes are shown in Fig. 5A–B for gray matter of healthy controls. High correlations (Pearson's correlation coefficient, i.e. the coefficient of determination, $R^2 = 0.61$ and 0.31, respectively) are found for the relationship between HC-BOLD and ALFF, and for the relationship between HO-BOLD and ALFF, respectively. This indicates that a substantial portion of the spatial variation in ALFF can be explained by HC/HO-BOLD. Knowing that HO-BOLD may act as a proxy for vCBV, these results imply that 31% of the spatial variation in ALFF may be explained by variation in vCBV. Furthermore, in Fig. 5C we demonstrate that, in healthy controls, 53% of the variation in HC-BOLD is subsequently explained by HO-BOLD. When normalizing the ALFF by total amplitude across all frequencies (fALFF), the variation explained by HC-BOLD reduces to 42% but still 29% of variation may be explained by vCBV (HO-BOLD). Table 2 shows all correlation results for both controls and occlusion patients, and for both ALFF and fALFF. Of importance, the correlation (R^2) between HC-BOLD and ALFF/fALFF drops to 0.33 and 0.15 in occlusion patients. As well, of the spatial variation in (f)ALFF a substantial portion (~14%–~31%) may be explained by the vCBV for which the HO-BOLD acts as a proxy.

Significant differences in kurtosis and variance of time delay distribution time delay were found between patients and controls in both gray and white matter (see Fig. 6A and 6B). Occlusion patients showed lower time delay kurtosis and higher variance, suggesting a wider range in blood arrival times owing to the ICA occlusion, consistent with the expectation that affected regions will prolonged HC induced BOLD response delays.

The HC-BOLD response to progressive hypercapnia for controls and patients with ICA occlusion is shown in Fig. 7. Global reductions in CVR are observed in individuals with occlusions where the difference in % BOLD, and consequently the effect size, increases for higher levels of $EtCO_2$. Simple main effect analysis showed that the gray matter HC-BOLD ramp response between patients and controls was significantly different ($F(1, 18) = 5.74$, $p = 0.028$). Subsequent post-hoc pairwise comparisons, Bonferroni adjusted, revealed that the HC-BOLD ramp response was significantly different at $\Delta EtCO_2$ values above and including +2 mmHg (at +2 mmHg $F(1, 18) = 5.85$, $p = 0.026$, see Fig. 7). No significant difference between patients and controls was found for white matter

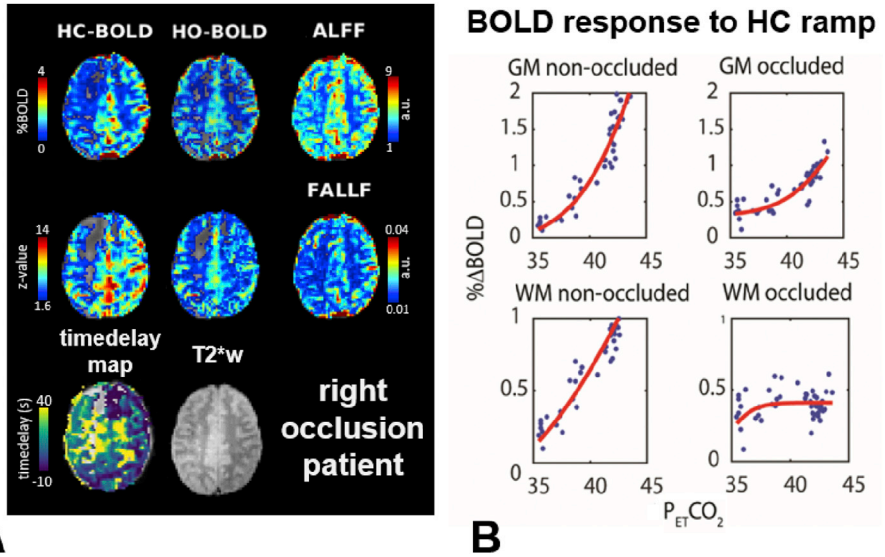

Fig. 2. Right occlusion patient example. (A) HC-BOLD, HO-BOLD, ALFF, fALFF and time delay map for a right occlusion patient, a single slice is shown. Reduced HC-BOLD and prolonged time delays in the left hemisphere whereas for the HO-BOLD, ALFF and ALFF no clear interhemispheric differences are observed. Note also the reduced HC- and HO-BOLD values in large draining veins areas for the z-value measure. (B) The effect of right occlusion is also apparent in the BOLD signal response to progressive hypercapnia with pronounced reductions in the response amplitude in both GM and WM regions ipsilateral to occlusion. Prolonged time delays in GM manifest as delayed onset in BOLD response (B – top right) as a stronger HC stimulus is required to increase vessel diameter in presumably pre-dilated regions (Halani et al., 2015).

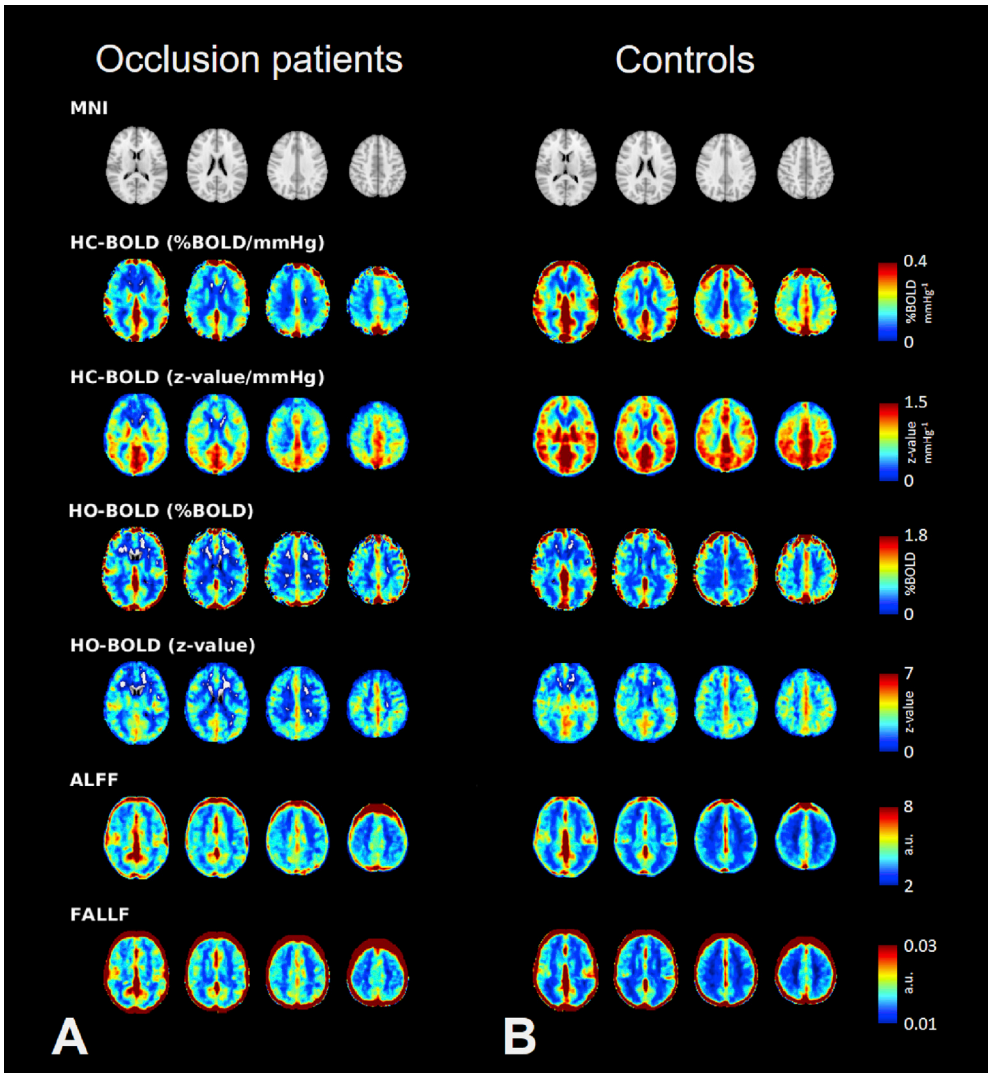

Fig. 3. Group average maps of HC-BOLD (%BOLD/mmHg, and z-value/mmHg), HO-BOLD (%BOLD and z-value), ALFF and fALFF for (A) occlusion patients, and (B) age and gender matched healthy controls. Images are shown in radiological convention and have been flipped where necessary to project the occlusion side on the right hemisphere. Both bilateral and unilateral occlusion patients are grouped in these images, grouped images demonstrating solely unilateral occlusion patients can be found in Supplemental Fig. 1. Differences in HC-BOLD between patients and controls are most apparent. For both the %BOLD as the z-value measure; note the reduction in high HC-BOLD values in large draining vein areas for the z-value HC- and HO-BOLD maps.

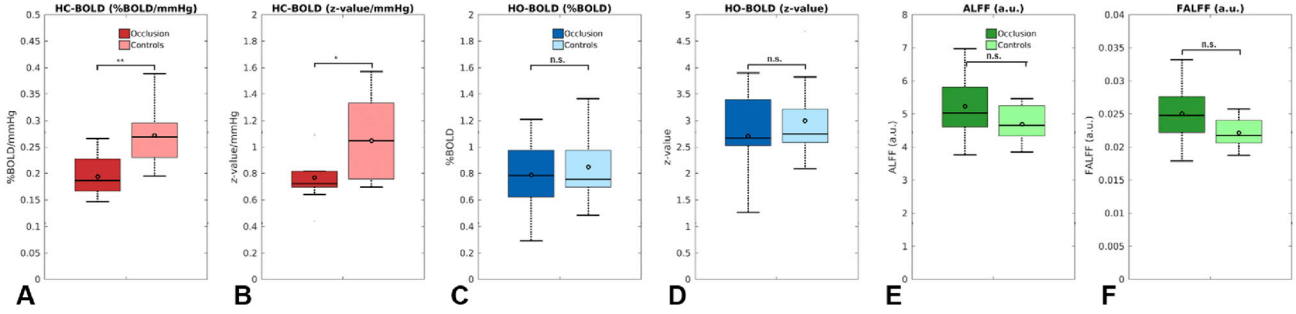

Fig. 4. Box plots showing the results for gray matter between occlusion patients and age and gender matched healthy controls for (A) HC-BOLD (%BOLD/mmHg), (B), HC-BOLD (z-value/mmHg), (C) HO-BOLD (%BOLD), (D) HO-BOLD (z-value), (E) ALFF, and (F) fALFF. Occlusion patients showed reduced HC-BOLD (both %BOLD/mmHg as z-value/mmHg) compared to control subjects. No apparent differences were found for the HO-BOLD, ALFF and fALFF measures. ** and * denote significant differences for $P < 0.005$ and $P < 0.05$ respectively for a one-sided Student's t-test.

tissue ($F(1, 18) = 2.67$, $p = 0.077$). The mixed design analysis (three way ANOVA with $\Delta EtCO_2$, tissue type and group type as the dependent variables) demonstrated a significant interaction for the HC-BOLD response between group type (patients, controls) and $\Delta EtCO_2$ ($F(1.74, 162) = 3.61$, $p = 0.045$). This means that the difference in %BOLD HC-BOLD between occlusion patients and healthy controls depends on the level of administered $EtCO_2$.

Table 3 shows the computed effect sizes (Cohen's d) for the HC-BOLD (%BOLD and z-value), HO-BOLD (%BOLD and z-value), ALFF, fALFF, time delay kurtosis, time delay variance and BOLD response to a progressive hypercapnia stimulus. Of all considered measures, the HC-BOLD and time delay kurtosis and time delay variance show the largest effect size for hemodynamic impairment (>1.11, i.e. large to very large effect size), closely followed by BOLD response to a progressive hypercapnia stimulus (large effect size of 0.9). The effect sizes of ALFF and fALFF are moderate (<0.712) while the effect size of HO-BOLD is small.

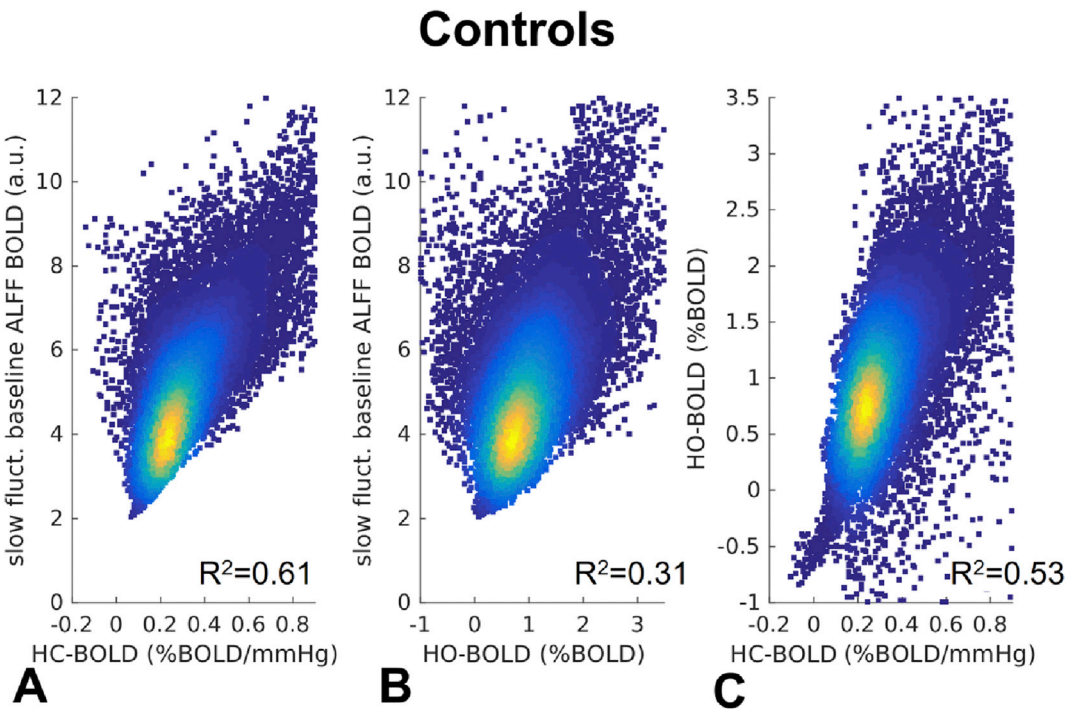

Fig. 5. For healthy controls, scatter plots of (A) HC-BOLD versus baseline low-frequency fluctuations ALFF, (B) HO-BOLD versus ALFF, and (C) HC-BOLD versus HO-BOLD. The Pearson correlation coefficient, i.e. coefficient of determination (R (Blaser et al., 2002)) are depicted in the bottom-right corners. High correlations are found for all three measures. Of the spatial variation in HC-BOLD and ALFF a substantial portion (~31%) can be explained by the baseline venous CBV for which the HO-BOLD acts as a proxy. Data points are from gray matter regions.

Table 2
Coefficient of determination R^2 of HC- and HO-BOLD versus baseline BOLD fluctuations ALFF and fALFF obtained by Pearson correlation.>

	Study group	HC-BOLD vs. ALFF	HO-BOLD vs. ALFF	HC-BOLD vs. HO-BOLD	HC-BOLD vs. fALFF	HO-BOLD vs. fALFF
R^2	controls	0.61	0.31	0.53	0.42	0.29
	occlusion patients	0.33	0.23	0.37	0.15	0.14

Coefficient of determination R^2 of HC and HO-BOLD versus baseline BOLD fluctuations ALFF and fALFF in gray matter obtained by Pearson correlation. Of the spatial variation in HC-BOLD and (f)ALFF a substantial portion (~14%–~31% for occlusion patients and healthy controls respectively) can be explained by the baseline venous CBV for which the HO-BOLD acts as a proxy. HC = hypercapnia, HO = hyperoxia, ALFF = amplitude of low-frequency fluctuations, fALFF = fractional amplitude of low-frequency fluctuations, BOLD = blood oxygenation level-dependent.

Discussion

In this study, different hemodynamic BOLD MRI -based measures were compared in patients with cerebrovascular disease and healthy controls. In particular, their effect sizes in determining hemodynamic impairment were evaluated. Comparable to earlier studies, a moderate relation between slow fluctuating BOLD signal, i.e. ALFF, and hypercapnia-assessed hemodynamic impairment was found. ALFF did not significantly differ in between patients and controls, and ALFF only demonstrated a moderate effect size to detect hemodynamic impairment. This contrasted with the large effect size seen using hypercapnia-based hemodynamic assessment methods. In addition, based on our analysis of BOLD signal change as a response to a progressively increasing hypercapnia stimulus we can argue that a hypercapnia stimulus of at least 2 mmHg above baseline $EtCO_2$ is necessary to evaluate hemodynamic impairment. Up to 31% of the variance in the ALFF spatial distribution could be explained by the HO-BOLD spatial distribution, which was regarded a proxy for baseline venous CBV. These findings confirm that a substantial amount of the information imbedded in the rsBOLD signal, and the HC-BOLD signal (53% of the spatial variation), is strongly weighted by the baseline cerebral venous blood volume (vCBV).

The basis for investigating rsBOLD as a means to evaluate cerebral hemodynamics was established when rsBOLD signals were shown to have a relationship with $EtCO_2$ (Wise et al., 2004; Chang and Glover, 2009). This finding lead to the presumption that breathing-related changes in arterial CO_2 concentration pose small vasodilatory challenges, which result in concomitant fluctuations of the BOLD signal. Initial studies comparing rsBOLD to breath-hold BOLD CVR were promising ($R^2 > 0.57$)[18], and similar relationships were found with functional HC-BOLD ($r > 0.59$, i.e. $R^2 > 0.35$) (Kannurpatti et al., 2014). Furthermore, Liu et al. found a relationship between BOLD signal fluctuations in the frequency range of 0.02–0.04 Hz and variations in $EtCO_2$ (Liu et al., 2017a), and results from their study showed a reasonable spatial agreement between rsBOLD and HC-BOLD maps ($r = 0.71$, i.e. $R^2 = 0.50$) (Liu et al., 2017a). The previous reports were supported by our control subjects, where a similar relationship between rsBOLD amplitude of low frequency fluctuations (ALFF) and HC-BOLD was found. However, this relation was attenuated in occlusion patients (from an R^2 of 0.61 in controls to 0.33 in patients). The lower agreement found in our patient data as compared to the data of Liu et al. derived from patients with cerebrovascular disease may have been caused by differences in investigated BOLD frequency ranges (Liu et al., 2017a). In our data, we did not detect any significant differences in (f)ALFF between occlusion patients and controls, and this was reflected in a moderate effect size (0.61 for ALFF and 0.72 for fALFF) of rsBOLD MRI to detect hemodynamic impairment.

Compared with the rsBOLD data, the effect size for HC-BOLD was substantially higher compared to the rsBOLD results. Our results regarding the BOLD response to progressive hypercapnia may help to explain this finding. In this analysis, significant differences in the GM response were found only when the CO_2 stimulus reached 2 mmHg above resting values. Breathing related fluctuations in $EtCO_2$ values during

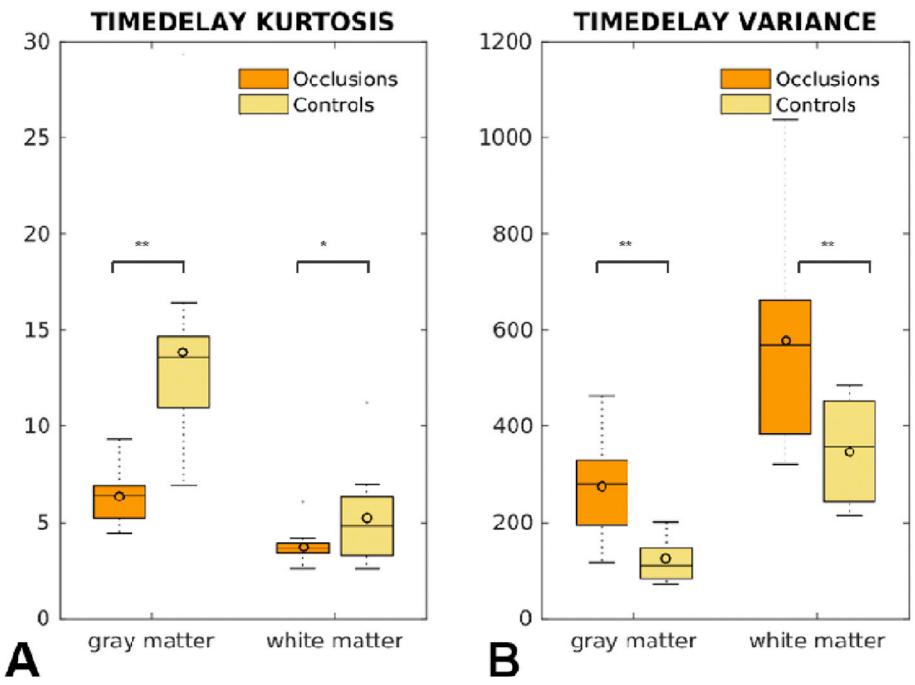

Fig. 6. Box plots showing the results between occlusion patients and age and gender matched healthy controls in gray and white matter for (A) kurtosis of the time delay distribution, and (B) variance of the time delay distribution. Lower kurtosis indicates a skewed time delay distribution containing a tail of prolonged time delays most likely as result of the ICA occlusion(s). The increased variance for the occlusion patients also reflects the higher time delay values in the distribution. ** and * denote significant differences for $P < 0.005$ and $P < 0.05$ respectively for a one-sided Student's t-test.

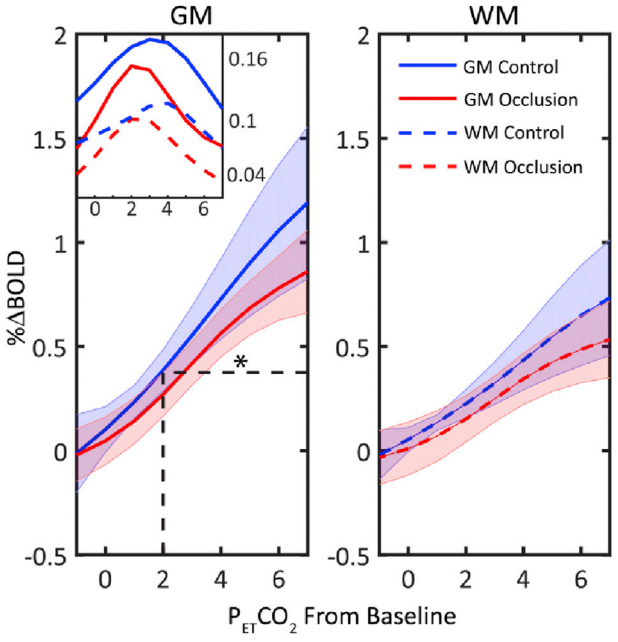

Fig. 7. The HC-BOLD response to progressive hypercapnia in GM (left panel) and WM (right panel) in controls (blue) and individuals with carotid artery occlusions (red). Global reductions in HC-BOLD are observed in individuals with occlusions. Inset top-right shows derivative curves of the HC-BOLD response. The HC-BOLD response in GM was significantly different starting from 2 mmHg above baseline $EtCO_2$. The WM HC-BOLD response showed no significant differences between patients and controls throughout the range of CO2 values sampled ($F(1, 18) = 2.67$, $p = 0.077$). * denotes the $\Delta EtCO_2$ values that showed significant differences in %BOLD between healthy controls and occlusion patients after post-hoc pairwise comparisons, Bonferroni adjusted. Mixed design analysis (ANOVA) demonstrated a significant interaction between group type (patients and healthy controls) and ΔEtCO2 ($F(1.74, 162) = 3.61$, $p = 0.045$), indicating that the difference in %BOLD between occlusion patients and healthy controls depends on the level of administered $EtCO_2$.

resting state measurements typically remain within 2 mmHg. Furthermore, it is known that the BOLD response to CO_2 follows a sigmoidal shape comprising a linear component about the resting vascular tone (Bhogal et al., 2014, 2015). Resting-state BOLD fluctuations are likely still around the linear regime of the response curve while HC-BOLD measurements integrate over the sigmoidal response curve and are thus more likely to detect mild to moderate hemodynamic impairment. Hence, it stands to reason whether basal $EtCO_2$ fluctuations are strong enough to act as a potent vascular stress stimulus and have a large enough effect size for detecting hemodynamic impairment, desirably already in a mild form. Besides the difficulties of rsBOLD MRI to detect hemodynamic impairment, we also demonstrated that a substantial amount of information imbedded in the ALFF was caused by baseline venous CBV (53% in case of healthy controls). After normalizing the ALFF by total amplitude across all frequencies (i.e. fALFF), purportedly to reduce large vessel contributions (Zou et al., 2008), vCBV still explained 29% of the variation in healthy controls. Therefore, care should be taken when attributing BOLD signal fluctuations such as (f)ALFF as a proxy for CO_2 vessel reactivity, especially in disease cases where cerebral blood volume can be compromised. As well, the reader should be aware that even though the set-up of a rsBOLD MRI sequence is less demanding, data-analysis is not straightforward yet and thus not readily applicable in clinical practice.

Findings from the rsBOLD analysis were also compared to time delay analysis and to the BOLD signal as a response to a progressively increasing hypercapnia stimulus. In line with the results reported by Donahue et al. (2015), our time delay analysis demonstrated a lower kurtosis and higher variance in patients with cerebrovascular disease (Donahue et al., 2015) with an effect size of 1.28 for time delay kurtosis and 1.56 for time delay variance. The effect size of the BOLD response to a progressively increasing hypercapnia stimulus (0.9) was large and a significant difference in GM response between occlusion patients and controls was found at +2 mmHg $EtCO_2$. This suggests that a shorter and less intense stimulus may be applied which would reduce scan time and possibly increase subject tolerance. Furthermore, this approach would eliminate the abrupt CO_2 increases associated with block hypercapnic stimuli which are thought to lead to a mixture of potentially confounding dynamic and static blood flow effects (Poublanc et al., 2015). An additional advantage of the BOLD response to a progressively increasing

Table 3
Effect sizes, Cohen's d, for comparison of the observed differences between occlusion patients and healthy controls in BOLD derived measures assessed in this study.

Effect size	HC-BOLD (% BOLD)	HC-BOLD (z-value)	HO-BOLD (% BOLD)	HO-BOLD (z-value)	ALFF	fALFF	time delay kurtosis	time delay variance	HC-BOLD ramp
Cohen's d	1.62	1.11	0.22	0.36	0.61	0.73	1.28	1.56	0.90

Effect sizes computed as the Cohen's d to quantify and compare the strength of the observed differences between occlusion patients and healthy controls in terms of HC-BOLD (%BOLD and z-value), HO-BOLD (%BOLD and z-value), ALFF, fALFF, time delay kurtosis and variance measures, and CVR response to a progressive increase in $EtCO_2$ (HC-BOLD ramp). Values below 0.5 are considered a small effect size, values above 0.8 and 1.2 are considered a large and very large effect size respectively (Sawilowsky, 2009).

hypercapnia stimulus is that it could determine the precise onset, and thus, the severity of the vascular impairment where HC-BOLD will be insensitive to this information. Furthermore, we did not observe a significant difference between patients and controls for the HC-BOLD response to progressive hypercapnia in white matter. However, considering a p-value of 0.077 and given the fact that we used a dual-echo MRI sequence which was not optimized for sensitivity to BOLD signal changes in white matter, there remains room for optimization in future MRI studies seeking to characterize white matter BOLD signal responses.

The findings described in this study have relevance with regard to the investigation of hemodynamic impairment in cerebrovascular disease, particularly the assessment of effect sizes. Effect sizes can be used to quantify and compare the strength of observed differences between two groups; in this case, occlusion patients and healthy controls (Sawilowsky, 2009). This information can be considered when designing clinical studies (power calculation and sample size planning) and when performing meta-analyses. However, when interpreting effect sizes a few limitations of the study should be considered. First, BOLD data gathered during respiratory modulation was used to obtain BOLD baseline signal changes in the baseline periods. Future studies could acquire resting-state BOLD MRI that employs longer baseline periods, and multi-slice and multi-echo acquisitions for higher temporal resolution and contrast-to-noise ratio. This may lead to larger effect sizes for ALFF and derived measures. Second, we focused on BOLD baseline signal changes within a frequency range of 0.01–0.08 Hz while Liu et al. have shown that the frequency range of 0.02–0.04 has the best relationship with $EtCO_2$. Additional analyses (see supplemental Table 1) on the narrower frequency range did not show any notable differences in R (Blaser et al., 2002) values related to the comparison between (f)ALFF and HC/HO-BOLD. However, we did note slightly smaller effect sizes for (f)ALFF with the narrow range which may be attributed to the reduced signal-to-noise ratio when narrowing the frequency range. With our approach, we did find a similar relationship between rsBOLD MRI and HC-BOLD for controls as Liu et al., but, not in the occlusion patients. Third, we derived vCBV from HO-BOLD and this measure may have been confounded by the disease state of our subjects (i.e. collateral circulation in patients with carotid occlusion). A more suitable measure for vCBV could be achieved with dynamic susceptibility contrast (DSC) MRI (Kuppusamy et al., 1996) or vascular space occupancy (VASO) MRI (Lu et al., 2003), although those techniques also have their limitations. For instance, DSC-derived CBV maps may be confounded by the arterial input function while quantitative VASO-based techniques may suffer from partial volume effects and differences in arterial arrival time which have to be properly corrected for using additional scans (Donahue et al., 2010; Hua et al., 2018).

Conclusion

Comparison of different BOLD-based hemodynamic assessment methods in patients with cerebrovascular disease and healthy controls demonstrated very large to large effect sizes for hypercapnia-based methods (conventional HC-BOLD, time delay analysis and the BOLD response to an increasing hypercapnic stimulus) to detect hemodynamic impairment. Progressively increasing HC has the advantage of providing secondary CVR information not available when solely applying a boxcar-type HC stimulus. In this case, it allowed us to estimate the minimum stimulus necessary to distinguish hemodynamic-impaired subjects from controls. A hypercapnia stimulus of at least 2 mmHg above baseline $EtCO_2$ was found to be necessary to depict hemodynamic impairment. Non-HC-based methods such as ALFF or fALFF only show moderate effect sizes and mainly seem to be confounded by resting CBV even though this must be confirmed in further studies. Our results indicate that vasoactive challenges are necessary to obtain reliable assessment of the brain's hemodynamic status.

Acknowledgements

The research of Jeroen Hendrikse has received funding from the European Research Council under the European Union's Horizon 2020 Programme (H2020) / ERC grant agreement n°637024 (HEART-OFSTROKE) and H2020 grant agreement No 666881, SVDs@target. We would like to thank Blaise de B Frederick for sharing and his assistance on the time delay RapidTiDe code.

Appendix A. Supplementary data

Supplementary data related to this article can be found at https://doi.org/10.1016/j.neuroimage.2018.06.017.

References

Bhogal, A.A., Siero, J.C.W., Fisher, J.A., et al., 2014. Investigating the non-linearity of the BOLD cerebrovascular reactivity response to targeted hypo/hypercapnia at 7T. Neuroimage 98, 296–305.
Bhogal, A.A., Philippens, M.E.P., Siero, J.C.W., et al., 2015. Examining the regional and cerebral depth-dependent BOLD cerebrovascular reactivity response at 7T. Neuroimage 114, 239–248.
Bhogal, A.A., De Vis, J.B., Siero, J.C.W., et al., 2016. The BOLD cerebrovascular reactivity response to progressive hypercapnia in young and elderly. Neuroimage 139, 94–102.
Biswal, B.B., Kannurpatti, S.S., 2009. Resting-state functional connectivity in animal models: modulations by exsanguination. Meth. Mol. Biol. 255–274.
Biswal, B., Yetkin, F.Z., Haughton, V.M., et al., 1995. Functional connectivity in the motor cortex of resting human brain using echo-planar MRI. Magn. Reson. Med. 34, 537–541.
Biswal, B.B., Kannurpatti, S.S., Rypma, B., 2007. Hemodynamic scaling of fMRI-BOLD signal: validation of low-frequency spectral amplitude as a scalability factor. Magn. Reson. Imaging 25, 1358–1369.
Blaser, T., Hofmann, K., Buerger, T., et al., 2002. Risk of stroke, transient ischemic attack, and vessel occlusion before endarterectomy in patients with symptomatic severe carotid stenosis. Stroke 33, 1057–1062.
Bulte, D., Chiarelli, P., Wise, R., et al., 2007. Measurement of cerebral blood volume in humans using hyperoxic MRI contrast. J. Magn. Reson. Imag. 26, 894–899.
Champagne, A.A., Bhogal, A.A., Coverdale, N.S., et al., 2017. A novel perspective to calibrate temporal delays in cerebrovascular reactivity using hypercapnic and hyperoxic respiratory challenges. Neuroimage. https://doi.org/10.1016/j.neuroimage.2017.11.044. Epub ahead of print 5 December.
Chang, C., Glover, G.H., 2009. Relationship between respiration, end-tidal CO2, and BOLD signals in resting-state fMRI. Neuroimage 47, 1381–1393.
Christen, T., Jahanian, H., Ni, W.W., et al., 2015. Noncontrast mapping of arterial delay and functional connectivity using resting-state functional MRI: a study in Moyamoya patients. J. Magn. Reson. Imag. 41, 424–430.
Christen, T., Jahanian, H., Ni, W.W., et al., 2015. Noncontrast mapping of arterial delay and functional connectivity using resting-state functional MRI: a study in Moyamoya patients. J. Magn. Reson. Imag. 41, 424–430.
Cogswell, P.M., Davis, T.L., Strother, M.K., et al., 2017. Impact of vessel wall lesions and vascular stenoses on cerebrovascular reactivity in patients with intracranial stenotic disease. J. Magn. Reson. Imag. 46, 1167–1176.
Conijn, M.M.A., Hoogduin, J.M., van der Graaf, Y., et al., 2012. Microbleeds, lacunar infarcts, white matter lesions and cerebrovascular reactivity — a 7T study. Neuroimage 59, 950–956.

Cox, R.W., 1996. AFNI: software for analysis and visualization of functional magnetic resonance neuroimages. Comput. Biomed. Res. 29, 162–173.
Davis, T.L., Kwong, K.K., Weisskoff, R.M., et al., 1998. Calibrated functional MRI: mapping the dynamics of oxidative metabolism. Proc. Natl. Acad. Sci. U. S. A. 95, 1834–1839.
De Vis, J.B., Petersen, E.T., Bhogal, A., et al., 2015. Calibrated MRI to evaluate cerebral hemodynamics in patients with an internal carotid artery occlusion. J. Cerebr. Blood Flow Metabol. 35, 1015–1023.
De Vis, J.B., Petersen, E.T., Bhogal, A., et al., 2015. Calibrated MRI to evaluate cerebral hemodynamics in patients with an internal carotid artery occlusion. J. Cerebr. Blood Flow Metabol. 35, 1015–1023.
Derdeyn, C.P., Grubb, R.L., Powers, W.J., 1999. Cerebral hemodynamic impairment: methods of measurement and association with stroke risk. Neurology 53, 251–259.
Donahue, M.J., Sideso, E., MacIntosh, B.J., et al., 2010. Absolute arterial cerebral blood volume quantification using inflow vascular-space-occupancy with dynamic subtraction magnetic resonance imaging. J. Cerebr. Blood Flow Metabol. 30, 1329–1342.
Donahue, M.J., Dethrage, L.M., Faraco, C.C., et al., 2014. Routine clinical evaluation of cerebrovascular reserve capacity using carbogen in patients with intracranial stenosis. Stroke 45, 2335–2341.
Donahue, M.J., Strother, M.K., Lindsey, K.P., et al., 2015. Time delay processing of hypercapnic fMRI allows quantitative parameterization of cerebrovascular reactivity and blood flow delays. J. Cerebr. Blood Flow Metabol. 36, 1767–1779.
Fierstra, J., Poublanc, J., Han, J.S., et al., 2010. Steal physiology is spatially associated with cortical thinning. J. Neurol. Neurosurg. Psychiatry 81, 290–293.
Frederick, B. deB., Nickerson, L.D., Tong, Y., 2012. Physiological denoising of BOLD fMRI data using Regressor Interpolation at Progressive Time Delays (RIPTiDe) processing of concurrent fMRI and near-infrared spectroscopy (NIRS). Neuroimage 60, 1913–1923.
Golestani, A.M., Wei, L.L., Chen, J.J., 2016. Quantitative mapping of cerebrovascular reactivity using resting-state BOLD fMRI: validation in healthy adults. Neuroimage 138, 147–163.
Halani, S., Kwinta, J.B., Golestani, A.M., et al., 2015. Comparing cerebrovascular reactivity measured using BOLD and cerebral blood flow MRI: the effect of basal vascular tension on vasodilatory and vasoconstrictive reactivity. Neuroimage 110, 110–123.
Hua, J., Liu, P., Kim, T., et al., 2018. MRI techniques to measure arterial and venous cerebral blood volume. Neuroimage. https://doi.org/10.1016/j.neuroimage.2018.02.027. Epub ahead of print.
Jahanian, H., Ni, W.W., Christen, T., et al., 2014. Spontaneous BOLD signal fluctuations in young healthy subjects and elderly patients with chronic kidney disease. PLoS One 9, e92539.
Jahanian, H., Christen, T., Moseley, M.E., et al., 2016. Measuring vascular reactivity with resting-state blood oxygenation level-dependent (BOLD) signal fluctuations: a potential alternative to the breath-holding challenge? J. Cerebr. Blood Flow Metabol. 37, 2526–2538.
Jenkinson, M., Smith, S., 2001. A global optimisation method for robust affine registration of brain images. Med. Image Anal. 5, 143–156.
Jenkinson, M., Bannister, P., Brady, M., et al., 2002. Improved optimization for the robust and accurate linear registration and motion correction of brain images. Neuroimage 17, 825–841.
Kannurpatti, S.S., Biswal, B.B., Kim, Y.R., et al., 2008. Spatio-temporal characteristics of low-frequency BOLD signal fluctuations in isoflurane-anesthetized rat brain. Neuroimage 40, 1738–1747.
Kannurpatti, S.S., Motes, M.A., Biswal, B.B., et al., 2014. Assessment of unconstrained cerebrovascular reactivity marker for large age-range fMRI studies. PLoS One 9, e88751.
Kuppusamy, K., Lin, W., Cizek, G.R., et al., 1996. In vivo regional cerebral blood volume: quantitative assessment with 3D T1-weighted pre- and postcontrast MR imaging. Radiology 201, 106–112.
Kuroda, S., Shiga, T., Ishikawa, T., et al., 2004. Reduced blood flow and preserved vasoreactivity characterize oxygen hypometabolism due to incomplete infarction in occlusive carotid artery diseases. J. Nucl. Med. 45, 943–949.
Lipp, I., Murphy, K., Caseras, X., et al., 2015. Agreement and repeatability of vascular reactivity estimates based on a breath-hold task and a resting state scan. Neuroimage 113, 387–396.
Liu, P., Li, Y., Pinho, M., et al., 2017. Cerebrovascular reactivity mapping without gas challenges. Neuroimage 146, 320–326.
Liu, P., Welch, B.G., Li, Y., et al., 2017. Multiparametric imaging of brain hemodynamics and function using gas-inhalation MRI. Neuroimage 146, 715–723.
Lu, H., Golay, X., Pekar, J.J., et al., 2003. Functional magnetic resonance imaging based on changes in vascular space occupancy. Magn. Reson. Med. 50, 263–274.
Mark, C.I., Slessarev, M., Ito, S., et al., 2010. Precise control of end-tidal carbon dioxide and oxygen improves BOLD and ASL cerebrovascular reactivity measures. Magn. Reson. Med. 64, 749–756.
Markus, H., Cullinane, M., 2001. Severely impaired cerebrovascular reactivity predicts stroke and TIA risk in patients with carotid artery stenosis and occlusion. Brain 124, 457–467.
Mazziotta, J., Toga, A., Evans, A., et al., 2001. A probabilistic atlas and reference system for the human brain: international Consortium for Brain Mapping (ICBM). Philos. Trans. R. Soc. Lond. B Biol. Sci. 356, 1293–1322.
Ogawa, S., Menon, R.S., Tank, D.W., et al., 1993. Functional brain mapping by blood oxygenation level-dependent contrast magnetic resonance imaging. A comparison of signal characteristics with a biophysical model. Biophys. J. 64, 803–812.
Poser, B.A., Versluis, M.J., Hoogduin, J.M., et al., 2006. BOLD contrast sensitivity enhancement and artifact reduction with multiecho EPI: parallel-acquired inhomogeneity-desensitized fMRI. Magn. Reson. Med. 55, 1227–1235.
Poublanc, J., Crawley, a. P., Fierstra, J., et al., 2011. Quantitative measurement of cerebrovascular reactivity by blood oxygen level-dependent MR imaging in patients with intracranial stenosis: preoperative cerebrovascular reactivity predicts the effect of extracranial-intracranial bypass surgery. Am. J. Neuroradiol. 32, 721–727.
Poublanc, J., Crawley, A.P., Sobczyk, O., et al., 2015. Measuring cerebrovascular reactivity: the dynamic response to a step hypercapnic stimulus. J. Cerebr. Blood Flow Metabol. 35, 1746–1756.
Poulin, M.J., Liang, P.J., Robbins, P.A., 1996. Dynamics of the cerebral blood flow response to step changes in end-tidal PCO2 and PO2 in humans. J. Appl. Physiol. 81, 1084–1095.
Sawilowsky, S., 2009. New effect size rules of thumb. Theor Behav Found Educ Fac Publ 8, 597–599.
Slessarev, M., Han, J., Mardimae, A., et al., 2007. Prospective targeting and control of end-tidal CO2 and O2 concentrations. J. Physiol. 581, 1207–1219.
Smith, S.M.B.J., 1997. SUSAN - a new approach to low level image processing. Int. J. Comput. Vis. 1, 45–78.
Sobczyk, O., Battisti-charbonney, A., Fierstra, J., et al., 2014. A conceptual model for CO2 -induced redistribution of cerebral blood flow with experimental confirmation using BOLD MRI. Neuroimage 92, 56–68.
Spano, V.R., Mandell, D.M., Poublanc, J., et al., 2013. CO $_2$ blood oxygen level–dependent MR mapping of cerebrovascular reserve in a clinical population: safety, tolerability, and technical feasibility. Radiology 266, 592–598.
Tong, Y., Frederick, B. deB., 2010. Time lag dependent multimodal processing of concurrent fMRI and near-infrared spectroscopy (NIRS) data suggests a global circulatory origin for low-frequency oscillation signals in human brain. Neuroimage 53, 553–564.
Wise, R.G., Ide, K., Poulin, M.J., et al., 2004. Resting fluctuations in arterial carbon dioxide induce significant low frequency variations in BOLD signal. Neuroimage 21, 1652–1664.
Yang, H., Long, X.-Y., Yang, Y., et al., 2007. Amplitude of low frequency fluctuation within visual areas revealed by resting-state functional MRI. Neuroimage 36, 144–152.
Yonas, H., Smith, H.A., Durham, S.R., et al., 1993. Increased stroke risk predicted by compromised cerebral blood flow reactivity. J. Neurosurg. 79, 483–489.
Zang, Y.-F., He, Y., Zhu, C.-Z., et al., 2007. Altered baseline brain activity in children with ADHD revealed by resting-state functional MRI. Brain Dev. 29, 83–91.
Zou, Q.-H., Zhu, C.-Z., Yang, Y., et al., 2008. An improved approach to detection of amplitude of low-frequency fluctuation (ALFF) for resting-state fMRI: fractional ALFF. J. Neurosci. Meth. 172, 137–141.